Hyperfine Interactions and Lifetimes of Low-Energy States in W^{182} and W^{183}†

D. AGRESTI, E. KANKELEIT,* AND B. PERSSON
California Institute of Technology, Pasadena, California
(Received 31 October 1966)

The Mössbauer technique has been used to study the nuclear hyperfine interactions and lifetimes in W^{182}(2^+ state) and W^{183}($\frac{3}{2}^-$ and $\frac{5}{2}^-$ states) with the following results: $g(\frac{5}{2}^-)/g(2^+)=1.40\pm0.04$; $g(\frac{3}{2}^-)=-0.07\pm0.07$; $Q(\frac{5}{2}^-)/Q(2^+)=0.94\pm0.04$; $T_{1/2}(\frac{3}{2}^-)=0.184\pm0.005$ nsec; $T_{1/2}(\frac{5}{2}^-)\gtrsim0.7$ nsec. These quantities are discussed in terms of a rotation-particle interaction in W^{183} due to Coriolis coupling. From the measured quantities and additional information on γ-ray transition intensities, magnetic single-particle matrix elements are derived. It is inferred from these that the two effective g factors, resulting from the Nilsson-model calculation of the single-particle matrix elements for the spin operators s_z and s_+, are not equal, consistent with the proposal of Bochnacki and Ogaza. The internal magnetic fields at the tungsten nucleus were determined for substitutional solid solutions of tungsten in iron, cobalt, and nickel. With $g(2^+)=0.24$ the results are: H_{eff}(W-Fe)$=-715\pm10$ kG; $|H_{\text{eff}}$(W-Co)$|=360\pm10$ kG; $|H_{\text{eff}}$(W-Ni)$|=90\pm25$ kG. The electric field gradients at the tungsten nucleus were determined for WS_2 and WO_3. With $Q(2^+)=-1.81$ b the results are: for WS_2, $eq=-(1.86\pm0.05)\times10^{18}$ V/cm^2; for WO_3, $eq=(1.54\pm0.04)\times10^{18}$ V/cm^2 and $\eta=0.63\pm0.02$.

INTRODUCTION

THE present paper reports on Mössbauer-effect measurements of the hyperfine splittings of the 2^+ state in W^{182}, the $\frac{5}{2}^-$ and $\frac{3}{2}^-$ states in W^{183}, and of the lifetimes of the $\frac{5}{2}^-$ and $\frac{3}{2}^-$ states in W^{183}. Magnetic hyperfine patterns were measured with ferromagnetic absorbers magnetically aligned by external fields. By choosing appropriate field configurations certain lines could be deleted from the observed hyperfine patterns, and the accuracy of the interaction energies obtained could be improved. These measurements, together with an adopted value for the magnetic moment of the 2^+ state, provide a determination of the magnetic moment of the $\frac{5}{2}^-$ state and of the internal fields at the tungsten nucleus in dilute solutions of tungsten in iron, cobalt, and nickel. Using a 50-kG superconducting solenoid, the sign of the internal field in iron was also determined. From a study of the dependence of the observed width of the $\frac{3}{2}^-$–$\frac{1}{2}^-$ transition on the thickness of tungsten, tungsten-nickel, and tungsten-iron absorbers, the lifetime and the magnetic moment of the $\frac{3}{2}^-$ state were obtained.

The largest quadrupole splitting was observed for tungsten disulfide, but only partially resolved patterns were obtained. A deviation of the relative transition intensities from those expected for an absorber of randomly oriented crystallites was observed at liquid-helium temperature. The quadrupole interaction in tungstic oxide was also studied and a non-axially-symmetric electric field gradient was found. From these measurements and the known quadrupole moment of the 2^+ state, the quadrupole moment of the $\frac{5}{2}^-$ state and the electric field gradients at the tungsten nucleus in the mentioned compounds were determined.

The magnetic moments of the $\frac{5}{2}^-$ and the $\frac{3}{2}^-$ states and the lifetime of the $\frac{3}{2}^-$ state have been used together with other experimental results to evaluate some single-particle magnetic matrix elements by assuming the RPC model (rotation-particle interaction due to Coriolis coupling) for the W^{183} nucleus. These are interpreted to imply the necessity of two effective single-particle g factors, as has been proposed by Bochnacki and Ogaza.[1]

EXPERIMENT

Because of the high energies of the transitions investigated, cooling of both the source and absorber is required to obtain a measureable resonant absorption. Most of the experiments were therefore performed at liquid-helium temperature in a cryostat as shown in Fig. 1.

The cryostat consists basically of two coaxial cylindrical containers separated by an evacuated volume (10^{-7}–10^{-6} Torr). The outer container is made from an aluminum tube and the inner one from a thin (7-mil) stainless-steel sheet. The inner one is wrapped with about 40 layers of "super insulation," a submicron glass paper alternating with layers of $\frac{1}{2}$-mil aluminum foil. Care is taken to avoid contact between successive layers of foil. Each layer of aluminum foil is separately connected to the inner container above the helium level so that the outer foils are connected to the upper warmer part of the container. With this arrangement the heat content of the outgoing gas is efficiently used. At the top of the cryostat is placed a set of thin stainless-steel plates, which serve the double purpose of radiation shields and separators for a number of gas layers,

† This work was performed under the auspices of the U. S. Atomic Energy Commission. Prepared under Contract No. AT(04-3)-63 for the San Francisco Operations Office, U. S. Atomic Energy Commission.
* Present address: Institut für Technische Kernphysik, Darmstadt, Germany.

[1] Z. Bochnacki and S. Ogaza, Institute of Nuclear Physics, Cracow, Report No. 428/PL, 1965 (unpublished).

thereby reducing the convection. These reflector plates and the filling tubes are mounted to the plate covering the top of the cryostat. A center hole in this assembly allows the extended part of the drive system, containing the source and the absorber, to be easily inserted into the cryostat. The transducer itself rests on the top plate outside of the cryostat. With this simple and inexpensive construction of the cryostat, a helium consumption of 0.13 liter/h was achieved.

The transducer, the source, and the absorber are enclosed in a container that is easily removed from the cryostat. The lower extended part, the source tube, is made of thin-walled (10-mil) stainless steel. It is surrounded by the liquid helium. The drive motion is transmitted to the source by an extension rod ($\frac{1}{4}$-in.-diam, 6-mil-wall stainless-steel tube) which is centered by a spiral-shaped phosphor-bronze spring in the absorber holder. This in turn is firmly pressed to the source tube by a stiff spring. By pushing the easily accessible drive coil downward, the absorber holder is brought into the position where the centering spring is unextended. The container may be evacuated and filled with an exchange gas for heat transfer. A small carbon resistor mounted on the extension rod is used to monitor the temperature of the source and the absorber. Thin beryllium disks serving as windows for the γ rays are mounted in the bottom of the source tube and the cryostat. The ease with which the source and absorber may be removed from the cryostat, changed, and reinserted allows the use of strong sources.

For the magnetization of the absorber in a direction transverse to the γ-ray beam, a C-shaped permanent magnet was used, which provided a field of about 2.5 kG in the plane of a disk-shaped absorber. Longitudinal magnetic fields of up to 50 kG at the absorber were supplied by a superconducting solenoid. Current leads to the coil and the heater for the superconducting switch are passed through a long thin-walled stainless-steel tube and end in four annular contact surfaces that mate with the solenoid contacts. It is important to avoid contamination of the contacts with films of solid air or ice since the increased contact resistance causes unnecessary heating which results in excessive helium loss during the charging of the coil. Current to the coil up to 30 A is supplied by a simple transistor circuit powered by storage batteries.

A multichannel analyzer operating in the multiscalar mode was synchronized with the motion of the transducer, as has been described in detail elsewhere.[2] It provided a velocity of triangular waveform to within 0.3%, as determined from the error signal. The electromechanical drive was calibrated by measuring the velocity spectrum of a single-line Co^{57} source versus an absorber of Fe^{57} in Armco iron. Calibration spectra were measured with the source at 300, 77, and 4.2°K and the

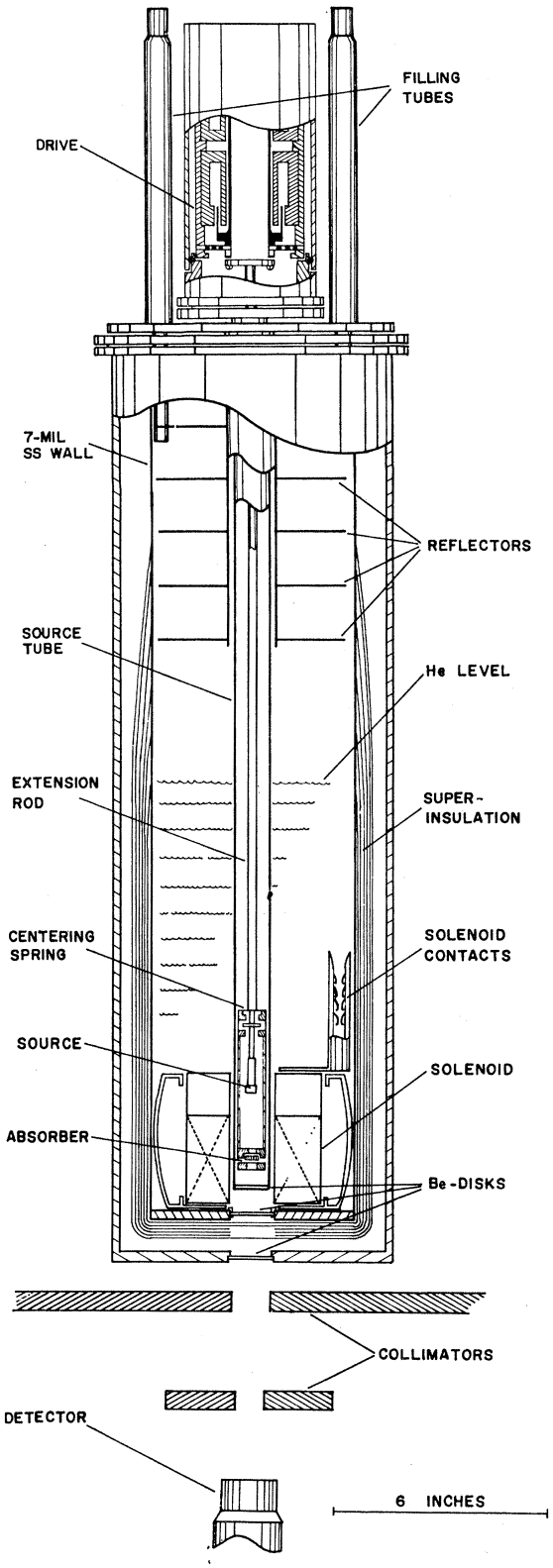

FIG. 1. Schematic diagram of the cryostat and the drive system used in the experiment.

[2] E. Kankeleit, Rev. Sci. Instr. **35**, 194 (1964); in *Mössbauer Effect Methodology*, edited by I. Gruverman (Plenum Press, Inc., New York, 1965), Vol. 1, p. 47.

absorber at room temperature. The relative positions of the lines were those of Preston *et al.*,[3] which were used as the standard, to better than 0.4%.

A sodium iodide scintillation detector ($1\frac{1}{2}$ in. × 1 in.) and a double-delay-line amplifier were used to detect the γ rays at a high counting rate. The detector was mounted close to the source, in the region of the strong stray field (≈0.5 kG) from the superconducting coil. The use of a light guide which decreases the resolution of the scintillation detector was thereby avoided. Instead, the photomultiplier was surrounded by a μ-metal mantle and a compensating coil. Adequate compensation could be provided, and almost the same resolution was obtained as in the absence of the stray field. The window of the single-channel analyzer, set for the relevant photopeak, contained for the 2^+–0^+ transition (100 keV) about 50% background from other lines and about 80 and 85% for the $\frac{5}{2}^-$–$\frac{1}{2}^-$ (99 keV) and $\frac{3}{2}^-$–$\frac{1}{2}^-$ (47 keV) transitions, respectively. The 47-keV line was enhanced by the use of a critical absorber of 180 mg/cm² Tb_4O_7. The precise position of the 47-keV photopeak was determined by recording the difference between pulse-height spectra obtained with and without recoilless absorption, i.e., with the source stationary and with the source oscillating with high velocity.

Sources for both the W^{182} and W^{183} measurements were produced by irradiation of tantalum metal in a neutron flux of 3.3×10^{14} n/cm² sec at the Materials Testing Reactor in Arco, Idaho. Both Ta^{182} and Ta^{183} were produced, and since the 100-keV line from the decay of Ta^{182} and the 99-keV line from the Ta^{183} decay cannot be separated by scintillation spectrometers, precautions had to be taken to avoid a simultaneous measurement of recoilless absorption in W^{182} and W^{183}. The sources were checked with a lithium-drifted germanium detector to determine the relative intensities of the two γ lines mentioned, and it was found that about 0.015 γ ray of 100-keV energy was emitted for every 99-keV γ ray at the time the source was removed from the reactor. The short lifetime of Ta^{183} (5.0 days) limited the time for which the sources could be used for the W^{183} measurements. Also, enriched absorbers had to be used for these measurements to reduce the W^{182} contribution in the velocity spectra to a negligible amount, viz., less than about 2% of the effect. Because of the comparatively long lifetime of Ta^{182} (115 days), sources for the W^{182} experiments were used after the Ta^{183} activity was reduced sufficiently by decay, and natural tungsten was used for the absorbers.

Absorbers for the experiments on the 99-keV transition in W^{183} were all made starting from enriched WO_3 (82.5% W^{183}; 6.4% W^{182}), and except for the W-Fe absorbers all were fine powder mixed with aluminum oxide powder to ensure uniform distribution. Tungsten metal powder was produced by the reduction of WO_3 in an atmosphere of hydrogen at 850°C. To make WS_2, a stoichiometric mixture of tungsten and sulphur in a pure nitrogen atmosphere was fused in a sealed quartz tube at 900°C.[4]

The alloy absorbers contained 1.8 at.% tungsten dissolved in ultrapure iron, cobalt, and nickel, except for the tungsten-iron absorbers used for the measurements on the 46.5-keV transition. These contained 3.6 at.% tungsten. It was verified that the internal fields were the same for the two concentrations of tungsten. The absorbers were prepared by pressing the tungsten powder into a small cavity in a pellet of the host material. By the use of a high-frequency field the pellet was levitated on a watercooled silver boat and melted in an argon atmosphere. The melt was kept for some time at about 1700°C to homogenize it. The alloy was shaped by repeated rolling and tempering in hydrogen to obtain disk-shaped absorbers, which were used mainly for measurements with transverse applied fields. For measurements without applied field and with longitudinal field, the absorbers were usually prepared by grinding the tempered alloy on a fine india stone and dispersing the powder (average grain size 3.5μ) in molten wax.

A tungsten-iron alloy produced with another technique gave a slightly smaller internal field. It was prepared by arc melting in an argon atmosphere and carefully annealing in hydrogen. Absorbers were also made of commercially obtained tungsten compounds of

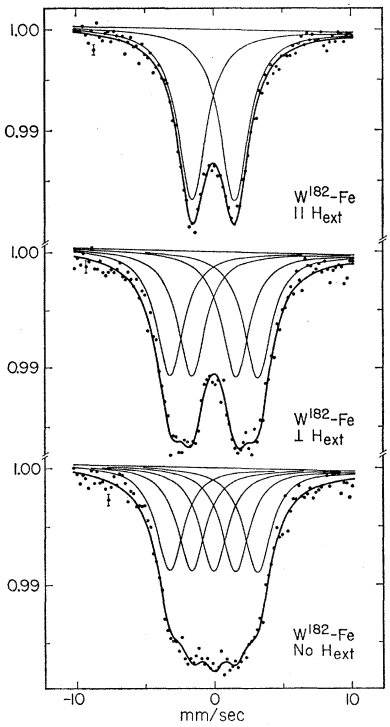

FIG. 2. Recoilless resonant absorption spectra for the 0^+–2^+ transition (100 keV) in W^{182} for tungsten dilutely dissolved in iron. The spectra correspond to various magnetic alignments of the absorber relative to the γ-ray beam. The slightly slanted base lines are caused by phase shifts in the pulse electronics.

[3] S. S. Hanna, R. S. Preston, and J. Heberle, in *The Mössbauer Effect*, edited by D. M. J. Compton and A. H. Schoen (John Wiley & Sons, Inc., New York, 1962), p. 85.

[4] O. Glemser, H. Sauer, and P. König, Z. Anorg. Allgem. Chem. **257**, 17 (1948).

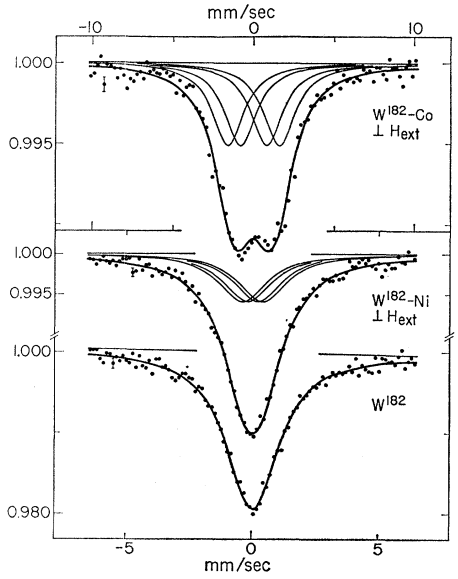

FIG. 3. Recoilless resonant absorption spectra for the 0^+–2^+ transition in W^{182} for absorbers of tungsten dilutely dissolved in cobalt and nickel and of tungsten-metal powder. The ferromagnetic absorbers were magnetized in a direction transverse to the γ-ray beam. The slightly asymmetric velocity pattern for W-Co may indicate presence of quadrupole interaction. A somewhat better fit to the spectrum was obtained assuming combined magnetic and quadrupole interaction. The quadrupole interaction may be appreciable, but it turns out that the value determined for the internal magnetic field is practically not affected.

reagent quality. All absorbers were carefully checked by x-ray and spectroscopic analysis for purity, proper composition, and crystalline structure.

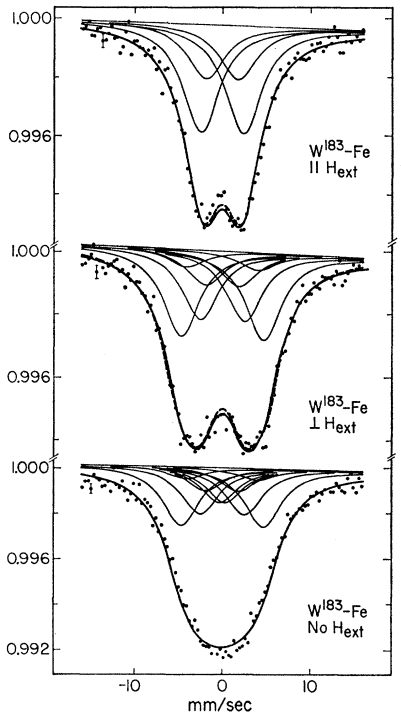

FIG. 4. Recoilless resonant absorption spectra for the $\frac{1}{2}^-$–$\frac{5}{2}^-$ transition (99 keV) in W^{183}. A disk-shaped absorber of enriched tungsten dilutely dissolved in iron was used. The solid curves are the fitted functions for three spectra simultaneously fitted by the least-squares method. The dashed curves correspond to the fit to the two spectra measured with applied fields.

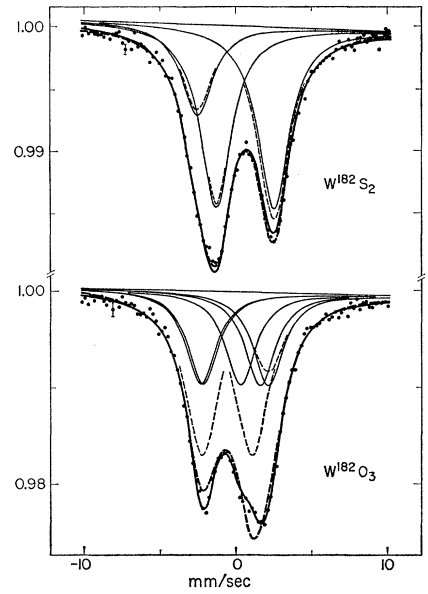

FIG. 5. Electric quadrupole patterns observed for the 0^+–2^+ transition in W^{182} for absorbers of tungsten disulfide and tungstic oxide. For WS_2, the solid curves correspond to the fit obtained with peak intensities fixed to the ratio 2:2:1, and the dashed curves are obtained with independently variable peak intensities. For WO_3, the solid curves correspond to the fit with variable asymmetry parameter η; the dashed curves are obtained with $\eta=0$.

ANALYSIS AND RESULTS

Examples of measured velocity spectra are shown in Figs. 2–6. The spectra were fitted on a computer to a sum of Lorentzian-shaped lines using the least-squares

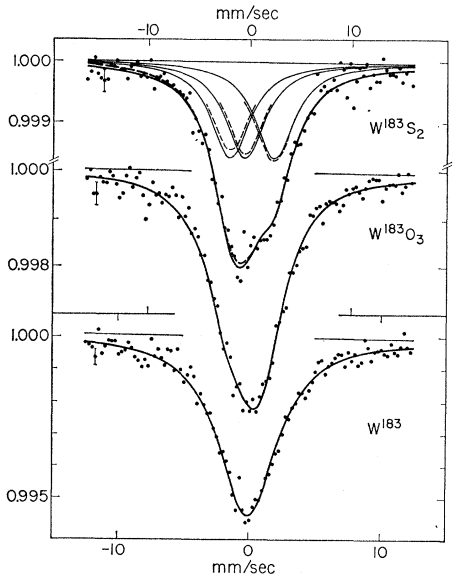

FIG. 6. Electric quadrupole patterns observed for the $\frac{1}{2}^-$–$\frac{5}{2}^-$ transition in W^{183} for absorbers of tungsten disulfide and tungstic oxide. Solid and dashed curves correspond to those in Fig. 5. The lower spectrum is obtained with an absorber of enriched tungsten-metal powder.

method. This is a good approximation of the true velocity spectrum for a source without self-absorption and absorbers of the thicknesses used, viz., less than the recoilless-resonant absorption length. A number of parameters, the number depending on the particular spectrum to be fitted, determine the positions, intensities, and widths of the lines.

A considerably improved determination of essential parameters, compared to what is obtained from the usual fitting of spectra individually, was achieved by a combined fitting procedure, in which several different spectra were analyzed together in one single least-squares procedure. Using this technique a parameter in the function assigned to fit any one of the spectra also might enter the function used to fit other spectra, e.g., the linewidth corrected for absorber thickness. If a combined fit of several spectra is possible, systematic errors might be revealed if present in one spectrum but not in the others. Also, spectra measured under different but complementary conditions and fitted together usually determine a common parameter more precisely than the same spectra fitted individually.

The spectra measured with a Ta^{182} source and tungsten-iron absorbers in various field configurations, shown in Fig. 2, were subjected to a combined fit by restricting the splitting of the excited state due to the internal field as well as the widths of the individual Lorentzians to be the same for all spectra. Small corrections for the effect of the external fields on the splittings and for the differences in the effective absorber thicknesses due to different spectrum shapes were taken into account. The relative intensities of the lines were restricted to that appropriate for a 2^+–0^+ transition, assuming the absorber to be completely demagnetized in the absence of an applied field and to be completely aligned by the action of one. The results of the fits are quoted in Table I. Individual fits to these spectra give results consistent with those of the combined fits, a fact which together with the good quality of the fits justifies the assumptions mentioned and gives no evidence for the presence of systematic errors. Adopting the value for the g factor of the 2^+ state, $g(2^+)=0.24$, an average of several recent measurements[5] and consistent with the value 0.25 calculated by Nilsson and Prior,[6] the internal field at the tungsten nucleus was determined. The internal fields in cobalt and nickel were determined in the same way; however, measurements were performed only with transverse applied field, and the velocity spectra are shown in Fig. 3. In order to determine the sign of the internal field at the tungsten nuclei in an iron lattice, the magnetic hyperfine spectra were measured for various applied longitudinal fields, up to 50 kG. The splitting was found to decrease for increased applied field, from which it is inferred that the internal field is directed opposite to the applied one.

The observed magnetic hyperfine patterns, shown in

TABLE I. Results from the study of the magnetic hyperfine interactions. Numbers within parentheses are standard deviations. The errors given are standard deviations increased to include the spread of the values and to take account of the uncertainties in the corrections as well as the precision of the velocity calibration.

Source	Absorber[a]	Thickness (mg W/cm²)	Fitted width (mm/sec)	Corrected width (mm/sec)	Excited-state splitting (mm/sec)	$\lvert H_{\text{int}}\rvert$[b] (kG)	$\lvert H_{\text{int}}\rvert/\mu_{\text{eff}}$[b,c] (kG/magneton)	Comments[d]	$\chi^2/(N-n)$
Ta^{182}	W-Fe	44	2.40±0.04	2.28	1.596±0.008	715±10	320	CF 0, ⊥, ∥	1.08±0.05
	W-Fe[e]	32	2.45±0.04	2.36	1.519±0.009	680±10		CF 0, ⊥, ∥	0.95±0.04
	W-Co	33	2.43±0.11	2.34	0.806±0.015	360±10	190	SF ⊥	1.19±0.14
	W-Ni	24	2.30±0.11	2.24	0.200±0.043	90±25	150	SF ⊥	1.43±0.14
	W	20	2.52±0.06	2.23				SLF	0.95±0.14
				2.30±0.06[f]					
					Ground-state splitting		$g(\frac{5}{2}^-)$[b,g]		
Ta^{183}	W*-Fe	48	4.90±0.20[h]	4.55	0.89 ±0.48	400±220	0.53 ±0.26	CF 0, ⊥, ∥[i]	1.19±0.05*
	W*-Fe	48	5.08±0.12[h]	4.73	1.57[j]		0.327±0.002	CF 0, ⊥, ∥	1.19±0.05*
	W*-Fe	48	5.12±0.12[h]	4.77	1.57[j]		0.338±0.002	CF ⊥, ∥	0.92±0.07*
	W*-Fe	48	4.62±0.15[h]	4.30	1.57[j]		−0.237±0.003	CF 0, ⊥, ∥[k]	1.47±0.05*
	W*	22	5.35±0.18	4.67				SLF	0.94±0.14*
				4.7 ±0.2[f]			0.34 ±0.01[f]		

[a] The symbol * stands for enriched material.
[b] The given values correspond to adopting $g(2^+)=0.24$, see text.
[c] μ_{eff} taken from Ref. 13.
[d] CF—Combined fit; SF—fit to a single velocity spectrum; SLF—fit to a single Lorentzian-shaped curve; 0—No applied field; ⊥—transverse applied field; ∥—longitudinal applied field.
[e] Alloy prepared by arc melting.
[f] The value is an average of the appropriate separate determinations.
[g] $g(\frac{5}{2}^-)$ is independent of the value of the width of the component Lorentzians. Fixing this width to values differing by as much as 30% does not affect $g(\frac{5}{2}^-)$.
[h] The quoted value corresponds to the spectra for the transverse-field configuration.
[i] Attempted determination of both the internal field and the g factor.
[j] Determined from the results for W^{182}.
[k] Attempted determination of a negative value for the g factor.

[5] For a recent compilation, see W. Ebert, O. Klepper, and H. Spehl, Nucl. Phys. 73, 217 (1965).
[6] S. G. Nilsson and O. Prior, Kgl. Danske Videnskab. Selskab, Mat. Fys. Medd. 32, No. 16 (1961).

TABLE II. Results from the study of quadrupole interactions.

Source	Absorber[a]	Fitted width[b] (mm/sec)	ce^2qQ/E_γ (mm/sec)	Electric field gradient[c] eq (10^{18} V/cm^2)	$Q(\frac{5}{2}^-)/Q(2^+)$	Relative peak intensities or asymmetry parameter	$\chi^2/(N-n)$[d]
Ta^{182}	WS_2	2.49±0.04	10.04±0.06			2:2:1[e]	1.58
		2.50±0.04	10.07±0.06	−1.86±0.05		2.12:1.96:0.93	1.01
	WO_3	2.84±0.08	−8.73±0.09			2:2:1[e]	8.18
		2.76±0.06	−8.23±0.10			2.12:1.41:1.47	4.25
		2.42±0.04	−8.34±0.05	+1.54±0.04		$\eta=0.63\pm0.02$	2.18
Ta^{183}	W^*S_2	4.8 ±0.3	9.45±0.40		0.931±0.038	1:1:1[e]	0.93
		4.7 ±0.3	9.55±0.38		0.939±0.036	1.06:0.99:0.95[e]	0.92
	W^*O_3	5.1 ±0.3	−7.92±0.37		0.940±0.050	$\eta=0.63$[e]	1.10

$Q(\frac{5}{2}^-) = -(1.70\pm0.07)$ b[c]

[a] The thicknesses were 50 mg W/cm^2 and 22 mg W*/cm^2, where the symbol * stands for enriched material.
[b] Not corrected for absorber thickness.
[c] Adopting $Q(2^+) = -(1.81\pm0.05)$ b, inferred from Coulomb-excitation experiments (Ref. 21).
[d] The standard deviation of $\chi^2/(N-n) \approx 0.14$ for all the fits.
[e] Kept fixed in the fitting procedure.

Fig. 4, for a Ta^{183} source and tungsten-iron absorbers in the various field configurations were subjected to a combined fit similar to that for the Ta^{182} spectra. The $\frac{5}{2}^- - \frac{1}{2}^-$ transition is of pure electric quadrupole character. A determination of both the internal field and the g factor of the $\frac{5}{2}^-$ state was attempted, but because of the strong correlation between the two parameters the fit was very little affected by a change in the value of either of them, and both parameters could not be accurately determined from the Ta^{183} measurements alone. Therefore, the internal field was fixed at the value determined from the Ta^{182} measurements, and as a consequence the value obtained for $g(\frac{5}{2}^-)$ depends on the adopted g factor of the 2^+ state in W^{182}. The ratio $g(\frac{5}{2}^-)/g(2^+)=1.40\pm0.04$ is, however, constant to well within the error for $g(2^+)$, within $0.2<g(2^+)<0.3$, and can be used to evaluate $g(\frac{5}{2}^-)$ when $g(2^+)$ has been consistently determined.

Since a disk-shaped solid absorber was used for the measurement without any applied field and an experiment with Ta^{182} and a solid absorber of similar shape indicated a partial magnetic alignment, a combined fit was performed excluding this Ta^{183} measurement. An improved fit and a somewhat different result was then obtained for the g factor of the excited state, as quoted in Table I. So far, only positive values for the g factor of the $\frac{5}{2}^-$ state have been considered. It is also possible to fit the present measurements with a negative g factor. The fit is, however, not so good as with the positive value, and the width of the fitted Lorentzians does not agree so well with the width determined for a tungsten absorber. Thus, a negative g factor seems less likely.

The observed quadrupole patterns for the transition in W^{182} are shown in Fig. 5. A deviation of the relative transition intensities from that expected for a polycrystalline absorber with randomly oriented crystallites is observed in the tungsten disulfide spectrum. The analysis of the velocity spectrum for the interaction energy was found, however, to be insensitive to the relative intensities of the peaks. A more pronounced deviation, opposite to that shown in Fig. 5, was found for a commercially obtained material. X-ray and spectroscopic analysis showed no difference between the two materials. In view of the exceptionally high magnetic susceptibility of tungsten disulfide, the measurements were repeated at 1.5°K with the absorber in a magnetic field of 50 kG to check on a possible magnetic interaction. No change in the anomalous spectrum was observed. At 77°K a quadrupole pattern with peak intensities in the expected ratio of 2:2:1 was obtained, which contradicts an explanation in terms of an anisotropic Debye-Waller factor.[7] So far, no explanation for this effect is available. The velocity spectrum obtained for a Ta^{183} source and an absorber of enriched tungsten disulfide shows very little structure, as seen from Fig. 6. Therefore, the analysis of this spectrum is not very sensitive to the ratio of the intensities of the peaks. Since the compound was prepared by the same technique as that for the W^{182} measurement, the relative intensities of the lines were inferred from that measurement and were kept fixed in the least-squares fitting procedure.

In view of the difficulties encountered in the study of the quadrupole interactions in tungsten disulfide, a similar study of tungstic oxide was performed to obtain an independent determination of the ratio of the two quadrupole moments involved. The symmetry at the site of the tungsten nucleus in tungstic oxide is known to be low and implies a non-axially-symmetric electric field gradient at the tungsten nucleus. As is demonstrated in Table II and Fig. 5, a reasonable fit to the measured velocity spectrum for the transition in W^{182} requires a large asymmetry parameter. In fitting

[7] S. V. Karyagin, Proc. Acad. Sci. USSR, Phys. Chem. Sect. 148, 110 (1964).

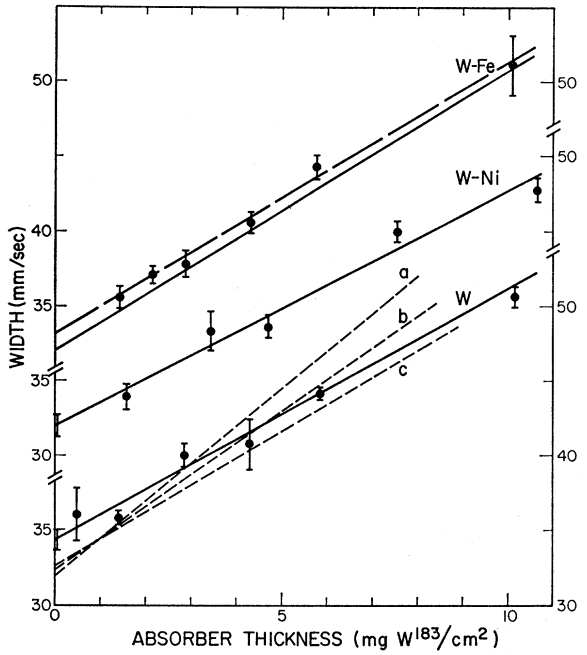

FIG. 7. The dependence of the measured width on the absorber thickness for the $\frac{1}{2}^-$–$\frac{3}{2}^-$ transition in W^{183} and absorbers of W, W-Ni, and W-Fe. Note the shifted scales for the widths. An experimental point indicates the width of the Lorentzian fitted to the measured velocity spectrum, and the error bars correspond to standard deviations. One measurement for W-Ni corresponding to the point (15.3; 55.9±2.4) is not shown in the diagram; the point falls exactly on the extension of the solid line. A solid line corresponds to the thickness dependence of the width of one single Lorentzian, determined by the combined fitting of all the measured velocity spectra for the particular absorber material. For W the dashed lines give the width dependence expected for solid tungsten absorbers. They were obtained by correcting the fitted solid line for granularity effects. The average grain size ($\approx 3.5\,\mu$) was measured and the following values were assumed for the Debye temperature (Θ_D) and for the total internal conversion coefficient (α_t): (a) $\Theta_D=360°K$, $\alpha_t=7.6$, (b) $\Theta_D=320°K$, $\alpha_t=8.4$, (c) $\Theta_D=280°K$, $\alpha_t=9.2$. For W-Fe the dashed line gives the width of the composite spectrum at half-maximum determined by the fit.

the velocity spectrum obtained for the transition in W^{183}, it was fixed and set equal to the value determined from the W^{182} experiment. The resulting ratio of the quadrupole moments is in good agreement with that determined from the tungsten disulfide experiments. No evidence for an isomeric shift has been found in the measurements reported here (upper limit: 0.05 mm/sec).

The widths obtained from the various experiments on the 2^+–0^+ transition in W^{182} are in good agreement with that observed using a tungsten metal absorber and the value 2.30±0.06 mm/sec can be quoted. A smaller value for this width, 2.0±0.2 mm/sec, has been quoted elsewhere[8]; the discrepancy might be due to source broadening and to some extent to noise produced by the boiling liquid. Correspondingly, there is good agreement among the widths determined for the $\frac{5}{2}^-$–$\frac{1}{2}^-$ transition in W^{183}. These widths do not, however, correspond to the natural width, because of source broadening. After the decay of Ta^{183} the source was checked in a W^{182} experiment. The width observed with an absorber of 20 mg W/cm² was 3.5 mm/sec. In spite of this broadening the spectrum shape was practically Lorentzian; hence the analysis of the W^{183} (99-keV) spectra in terms of Lorentzian components is justified. One can estimate the lifetime of the $\frac{5}{2}^-$ state by correcting for the source broadening by assuming it to be caused by distributed electric field gradients. Then the width is 3.9±0.4 mm/sec, which corresponds to the half-life $T_{1/2}(\frac{5}{2}^-)$ = 0.72±0.07 nsec.

A determination of the lifetime and the magnetic moment of the $\frac{3}{2}^-$ state in W^{183} was attempted from a study of the dependence of the absorption spectrum on the thickness of tungsten metal and tungsten-iron alloy absorbers. For absorbers of uniform thickness, the half-width of the nearly Lorentzian velocity spectrum is expected to depend linearly on the thickness of the absorber,[9] and the width corresponding to zero thickness can be determined by linear extrapolation, as demonstrated in Fig. 7. Fine powder (average grain size ≈0.5 and ≈0.02 recoilless-resonant absorption lengths for W and W-Fe, respectively) dispersed in wax was, however, used for the absorbers, and it was found for the tungsten measurements that the widths measured are affected by the absorber granularity to the extent that Visscher's formula[9] cannot be used to determine the natural linewidth. The effects of absorber granularity have been treated in detail elsewhere[10]; the correction to the extrapolated width is approximately proportional to the grain size measured in units of the recoilless-resonant absorption length. In Fig. 7 estimations of this correction to the tungsten measurements are indicated, from which it is inferred that the corresponding correction to the tungsten-iron measurements is negligible because of the much smaller grain size.

To avoid granularity effects, and since sufficiently thin tungsten metal foils could not be obtained, solid absorbers of tungsten-nickel alloy were used for the determination of the natural linewidth of the 46.5-keV transition. Line broadening due to magnetic interaction is negligible (cf. Table I). From a combined least-squares fit to the observed velocity spectra for six absorber thicknesses, restricting the fitted widths to be proportional to the thickness of the absorber, the width for zero absorber thickness was determined to 32.0±0.8 mm/sec, which corresponds to the half-life $T_{1/2}(\frac{3}{2}^-)$ = 0.184±0.005 nsec. Similarly, the velocity spectra obtained for tungsten-iron absorbers were fitted in one least-squares procedure. The value 32.0±0.8 mm/sec was taken for the width corresponding to zero absorber thickness, and the ground-state splitting was fixed to a

[8] E. Kankeleit, Z. Physik **164**, 442 (1961); S. G. Cohen, N. A. Blum, Y. W. Chow, R. B. Frankel, and L. Grodzins, Phys. Rev. Letters **16**, 322 (1966).

[9] W. M. Visscher, as quoted in H. Frauenfelder, *The Mössbauer Effect* (W. A. Benjamin, Inc., New York, 1962), p. 45.

[10] J. D. Bowman, E. Kankeleit, E. N. Kaufmann, and B. Persson, Nucl. Instr. Methods (to be published).

TABLE III. Magnetic moments, $B(M1)$ values, and magnetic parameters determined from these. The units for the magnetic moments and the $B(M1)$ values are nm and $(\text{nm})^2$, respectively. Column A gives the result of the fit with all parameters varied; column B corresponds to fixing the two parameters to which the fit is insensitive. Except where noted, the $B(M1)$ values are determined from the following quantities: (1) the ratio of the γ-ray intensity of the appropriate transition to that of the crossover transition originating from the same level (averaged from those of Refs. 22 and 23); (2) the $B(E2)$ value for the crossover transition (calculated from the values of $Q^{1/2,1/2}$ and $Q^{1/2,1/2}b_{E2}$ given in the text); and (3) the mixing ratio for the direct transition (Ref. 24).

Quantity	Experimental value	Predictions of Brockmeier *et al.*	Fits to present data A[a]	Fits to present data B
$\mu(\frac{1}{2}^-)$	0.117	0.123	0.117	0.117
$\mu(\frac{3}{2}^-)$	-0.1 ± 0.1	-0.28	-0.22	-0.08
$\mu(\frac{5}{2}^-)/\mu(2^+)$	1.75 ± 0.05	1.98	1.79	1.86
$B(M1, \frac{3}{2}^- \rightarrow \frac{1}{2}^-, 46.5)$[b]	0.209 ± 0.020	0.288	0.176	0.178
$B(M1, \frac{5}{2}^- \rightarrow \frac{3}{2}^-, 52.6)$	0.0239 ± 0.0017	0.0316	0.0256	0.0263
$B(M1, \frac{7}{2}^- \rightarrow \frac{5}{2}^-, 107.9)$	0.216 ± 0.029	0.245	0.193	0.164
$B(M1, \frac{5}{2}^- \rightarrow \frac{3}{2}^-, 82.9)$	$(0.94 \pm 0.26) \times 10^{-3}$	1.39×10^{-3}	0.98×10^{-3}	1.02×10^{-3}
g_R		0.24[c]	0.25 ± 0.04	0.28
$G^{1/2,1/2}$		-1.25	-1.06 ± 0.05	-1.06
$G^{1/2,1/2}b_{M1}$		-0.89	-0.74 ± 0.06	-0.70
$G^{1/2,3/2}$		-0.21	-0.04 ± 0.13	-0.21[d]
$G^{3/2,3/2}$		0.68	-0.2 ± 0.7	0.68[d]

[a] Errors given are standard deviations.
[b] Calculated from $T_{1/2}(\frac{3}{2}^-)$ with $\alpha_t = 8.4$ [L. A. Sliv and I. M. Band, in *Alpha-, Beta-, and Gamma-Ray Spectroscopy*, edited by K. Siegbahn (North-Holland Publishing Company, Amsterdam, 1965), p. 1639. The total internal conversion coefficient was estimated from $\alpha_t = 1.3\alpha_L$], and $\delta^2 = 0.006$ (Ref. 24).
[c] Adopted value, equal to g_R of the ground-state rotational band in W^{182}; Brockmeier *et al.* use $g_R = 0.35$.
[d] Fixed at the value predicted by Brockmeier *et al.* (Ref. 20).

value in accordance with the measured internal field. The magnetic moment of the $\frac{3}{2}^-$ state was then determined by the fit; $g(\frac{3}{2}^-) = -0.07 \pm 0.07$ or $g(\frac{3}{2}^-) = 0.2 \pm 0.2$. Only negative values for $g(\frac{3}{2}^-)$ are, however, consistent with other experimental quantities (cf. Table III). A fit to the W-Fe data with variable width for zero absorber thickness was also possible and gave values in agreement with the above, but with somewhat larger errors.

DISCUSSION

The internal magnetic field (715 ± 10 kG) at tungsten nuclei in dilute solution in iron determined in the present work is in agreement with that (700 ± 70 kG) obtained in an earlier Mössbauer experiment[11] but is inconsistent with the value (430 ± 100 kG) determined by the Coulomb excitation technique.[12] There is better agreement among the results of the present measurements of the internal fields for tungsten in cobalt (360 ± 10 kG) and nickel (90 ± 25 kG) and the fields obtained in Coulomb excitation experiments[12] (Co: 330 kG; Ni: 60 kG). Since vastly different concentrations of tungsten were used in the two types of experiments, a dependence of the field on the concentration may be the cause of the discrepancy. However, no such dependence was found for tungsten-iron alloys containing from 0.18 to 3.6 at.% tungsten. While the Mössbauer experiments were performed at low temperatures, the Coulomb-excitation measurements were done at room temperature. A reason for the different fields observed in the two types of experiments might be the existence of a local moment on the tungsten atom, due to which the temperature dependence of the internal field could be different from that of the host magnetization. Since Mössbauer experiments at sufficiently high temperatures cannot be performed, Coulomb-excitation experiments at low temperature would be of interest.

It is demonstrated in Table I that the ratio of the field and the host magnetic moment is not constant; thus the field does not depend on the host magnetic moment alone as has been suggested by Shirley and Westenbarger.[13] The variation of the internal field at an impurity nucleus of a transition element in an iron lattice has been discussed by Campbell.[14] By correlating measurements of the internal field with measurements of the local impurity moment he shows that the internal field may be represented by a sum of two terms, $H = a\mu_{\text{local}} + b\mu_{\text{host}}$, where μ_{local} is the impurity magnetic moment, μ_{host} is the host magnetic moment, and a and b are empirical constants. Similar measurements[15] of the field at platinum nuclei in iron, cobalt, and nickel also suggest that the field depends on the local moment as well as on the host moment.

The electric field gradient at the tungsten nucleus in tungsten disulfide agrees with an earlier measurement.[16]

[11] E. Kankeleit, Bull. Am. Phys. Soc. **10**, 65 (1965); the value has been recalculated using $g(2^+) = 0.24$.
[12] F. Boehm, G. B. Hagemann, and A. Winther, Phys. Letters **21**, 217 (1966); G. Goldring (private communication).
[13] D. A. Shirley and G. A. Westenbarger, Phys. Rev. **138**, A170 (1965).
[14] L. A. Campbell, Proc. Phys. Soc. (London) **89**, 71 (1966).
[15] D. Agresti, E. Kankeleit, and B. Persson, preceding paper, Phys. Rev. **155**, 1339 (1967).
[16] E. A. Phillips and L. Grodzins, in *Perturbed Angular Correlations*, edited by K. Siegbahn (North-Holland Publishing Company, Amsterdam, 1964), p. 294.

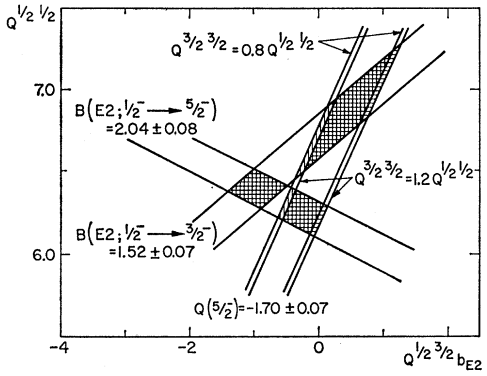

FIG. 8. Comparison of the electric parameters for W^{183} derived from the ratio of the quadrupole moments $Q(\frac{5}{2}^-)/Q(2^+)$ measured in the present experiment and $B(E_2)$ values measured by the Coulomb-excitation technique (Ref. 21). The ratio of the quadrupole moments and $B(E_2,\ 0^+-2^+)=4.00\pm0.20e^2b^2$ imply $Q(\frac{5}{2}^-)=-1.70\pm0.07$b. The three quantities $Q(\frac{5}{2}^-)$, $[B(E2;\frac{1}{2}^--\frac{3}{2}^-)]^{1/2}$, and $[B(E2;\frac{1}{2}^--\frac{5}{2}^-)]^{1/2}$ depend linearly on the quantities $Q^{1/2,1/2}$, $Q^{1/2,3/2}$, $Q^{1/2,3/2}b_{E2}$, and $Q^{3/2,3/2}$. It is assumed that $Q^{1/2,3/2}=0$; also $Q^{3/2,3/2}$ enters only in $Q(\frac{5}{2}^-)$ and is therefore of little importance.

In tungsten oxide it was found to be highly non-axially-symmetric, contradicting previous results.[17]

The level structure and the γ-ray transition intensities in the strongly deformed W^{183} nucleus cannot be well accounted for by an adiabatic rotational model for the nucleus. A significantly improved description was obtained by Kerman[18] as the result of mixing of states in the two low-lying bands, $K=\frac{1}{2}$ and $\frac{3}{2}$, by Coriolis coupling (the RPC model). More extensive band mixing has been considered by Rowe[19] and by Brockmeier *et al.*[20]; the results of the latter work, viz., the mixing parameters and the magnetic matrix elements, and its notation, will be used in the following comparison of the experimental results with calculations in terms of the RPC model. Since the admixture of states of the higher bands into the low-lying levels is very small, mixing of states in only the two lower bands is considered. Thus the moments and the $M1$ and $E2$ transition probabilities can be described by the following eight matrix elements: $G^{1/2,1/2}$, $G^{1/2,1/2}b_{M1}$, $G^{1/2,3/2}$, $G^{3/2,3/2}$, and $Q^{1/2,1/2}$, $Q^{1/2,3/2}$, $Q^{1/2,3/2}b_{E2}$, $Q^{3/2,3/2}$, where $G^{KK}=K(g_K-g_R)$ and $b_{M1}=b_0\sqrt{2}$.

The accurately determined ratio of the quadrupole moments, $Q(\frac{5}{2}^-)/Q(2^+)=0.94\pm0.04$, suggests a comparison with accurately measured $B(E2)$ values for Coulomb excitation in W^{182} and W^{183},[21] presented in Fig. 8. These measurements are just barely consistent, possibly due to underestimation of errors, but the diagram allows the determination of $Q^{1/2,1/2}=6.5\pm0.3$ b and $Q^{1/2,3/2}b_{E2}=-0.4\pm0.5$ b.

The measured magnetic moments, $\mu(\frac{3}{2}^-)$ and $\mu(\frac{5}{2}^-)$, and the measured half-life of the $\frac{3}{2}^-$ state can be compared with values derived from the magnetic parameters of Brockmeier *et al.* The latter were obtained from the fit to a large number of relative γ-ray transition intensities[22] with the assumption $Q^{1/2,1/2}=6.5$ b, which agrees with the value determined above. To calculate the magnetic moments, the g factor for the core rotation g_R must be assumed and is here taken equal to the g factor of the ground-state rotational band of W^{182}, since the contribution to g_R from the odd neutron has been accounted for in the band-mixing theory. Contributions to g_R due to higher bands and blocking effects are small compared to the uncertainty in the g factor of W^{182}. The comparison is presented in Table III. It is seen that $\mu(\frac{1}{2}^-)$ is well accounted for, but $\mu(\frac{3}{2}^-)$, $\mu(\frac{5}{2}^-)$, and $B(M1;\ \frac{3}{2}^--\frac{1}{2}^-)$ differ from the predictions of Brockmeier *et al.*

Recently, new experimental information on the W^{183} nucleus has become available,[23,24] which, together with the results of the present experiment, calls for a redetermination of the magnetic single-particle matrix elements. The data used in addition to the results of the present measurements and the value of the ground-state magnetic moment are those $B(M1)$ values for transitions of predominantly magnetic character that can be determined most precisely. In Table III are listed the experimental quantities used. These are fitted by the theoretical magnetic transition rates and moments[20] with the least-squares method. The fit is found to be insensitive to the parameters $G^{1/2,3/2}$ and $G^{3/2,3/2}$. The influence of constraints on these parameters was investigated to determine the reliability of the values obtained for the parameters g_R, $G^{1/2,1/2}$, and $G^{1/2,1/2}b_{M1}$; the results of such a fit are also included in the table. It was also checked that these latter parameters do not depend sensitively on any individual experimental quantity. The following values can be quoted:

$$g_R=0.25\pm0.04,$$
$$G^{1/2,1/2}=-1.06\pm0.05,$$
$$G^{1/2,1/2}b_{M1}=-0.74\pm0.06.$$

According to the Nilsson model the matrix elements $G^{1/2,1/2}$ and $G^{1/2,1/2}b_{M1}$ are given by the expressions:

$$G^{1/2,1/2}\equiv\tfrac{1}{2}(g_K-g_R)=(g_l-g_R)\langle\tfrac{1}{2}|\mathbf{j}_z|\tfrac{1}{2}\rangle + (g_s{}^z-g_l)\langle\tfrac{1}{2}|\mathbf{s}_z|\tfrac{1}{2}\rangle,$$

$$G^{1/2,1/2}b_{M1}\sqrt{2}\equiv(g_K-g_R)b_0=(g_l-g_R')\langle\tfrac{1}{2}|\mathbf{j}_+|-\tfrac{1}{2}\rangle + (g_s{}^+-g_l)\langle\tfrac{1}{2}|\mathbf{s}_+|-\tfrac{1}{2}\rangle,$$

[17] N. Sikazono, H. Takekoshi, and T. Shoji, J. Phys. Soc. Japan **20**, 271 (1965).
[18] A. K. Kerman, Kgl. Danske Videnskab. Selskab, Mat. Fys. Medd. **30**, No. 15 (1956).
[19] D. J. Rowe, Nucl. Phys. **61**, 1 (1965).
[20] R. T. Brockmeier, S. Wahlborn, E. J. Seppi, and F. Boehm, Nucl. Phys. **63**, 102 (1965).
[21] O. Hansen, M. C. Olesen, O. Skilbreid, and B. Elbek, Nucl. Phys. **25**, 634 (1961).
[22] W. F. Edwards, F. Boehm, J. Rogers, and E. J. Seppi, Nucl. Phys. **63**, 97 (1965).
[23] U. Gruber, R. Koch, B. P. Maier, and O. W. B. Schult, Z. Naturforsch. **20a**, 929 (1965).
[24] P. Alexander and R. S. Hager, Phys. Rev. **139**, B288 (1965).

where, in the strict sense of the model, $g_s^z = g_s^+ = g_s$, the free-nucleon value, and $g_R' = g_R$. It is well known that the interaction between the spin of the odd nucleon and the spins of the nucleons in the core reduces the spin contribution to the nuclear magnetic moment and that this effect can be accounted for by the use of an effective value in place of g_s. The spin operators $\mathbf{s}_z$ and $\mathbf{s}_+$ are then acting on the unchanged single-particle states. Furthermore, it has recently been pointed out by Bochnacki and Ogaza[1] that the spin polarization in the direction parallel to the symmetry axis of the nucleus might not be the same as that in a direction transverse to the symmetry axis. One may therefore not assume that g_s^z and g_s^+ are equal. The matrix element $\langle \frac{1}{2} | \mathbf{j}_+ | -\frac{1}{2} \rangle$ is only slightly affected by the spin polarization, so that $g_R' \approx g_R$.[1] Knowledge of the value of g_R' is, however, not necessary since the term in which it appears does not have to be evaluated from the model, but can be obtained from the experimentally determined[20] decoupling parameter $a_0 = -\langle \frac{1}{2} | \mathbf{j}_+ | -\frac{1}{2} \rangle$. The matrix elements have been evaluated using $g_l = 0$, various assumptions for the potential, and adopting $g_R = 0.24$. The effective single-particle g factors g_s^z and g_s^+ are then obtained by comparison with the experimental values for $G^{1/2,1/2}$ and $G^{1/2,1/2} b_{M1}$ and are quoted in Table IV.

For comparison, corresponding values for Yb^{171} and Tm^{169} have been calculated from available experimental data.[25–27] Since the primary experimental results have not been analyzed in terms of band mixing, one should in principle correct for its effects on the experimental quantities g_K, g_R, and b_0.[28,29] Such corrections have been estimated by assuming only $K = \frac{3}{2}$ bands to mix with the $K = \frac{1}{2}$ ground state.[28] One consequence of the neglect of mixing with $K = \frac{1}{2}$ bands is that no correction is obtained for the quantity $(g_K - g_R) b_0$. In Table IV are given the results of two calculations of the effective g factors g_s^z and g_s^+, one accounting for Coriolis mixing with the $K = \frac{3}{2}$ bands only and the other without Coriolis mixing.

Table IV. Effective single-particle g factors derived from the results of the present experiment (W^{183}) and from the experimental data of Refs. 26 and 27 (Yb^{171}) and of Ref. 25 (Tm^{169}). The matrix elements of the spin operators have been calculated from recent Nilsson wave functions (Ref. 28), using the potential parameters $\kappa = 0.0637$ and $\mu = 0.42$. The errors quoted are derived from the uncertainties in the experimental data only.

Quantity	W^{183}	Yb^{171}	Tm^{169}
$\langle \frac{1}{2} \lvert \mathbf{s}_z \rvert \frac{1}{2} \rangle$	0.281	−0.183	−0.356
$\langle \frac{1}{2} \lvert \mathbf{s}_+ \rvert -\frac{1}{2} \rangle$	0.781	0.317	−0.144
g_s^z/g_s	0.88±0.04	[a] 1.01±0.02 [b] 0.95±0.09	[a] 0.83±0.02 [b] 0.76±0.03
g_s^+/g_s	0.37±0.03	[a] 0.60±0.01 [b] 0.64±0.03	[a] 0.39±0.05 [b] 0.51±0.05

[a] Without correction for Coriolis mixing.
[b] Corrected for Coriolis mixing with $K = \frac{3}{2}$ band.

It is demonstrated in the table that for both assumptions the values derived from g_s^z and g_s^+ using recent Nilsson wave functions[30] differ from each other significantly. It should be pointed out that the values calculated for the effective g factors depend on the potential used in the nuclear model. If the old Nilsson wave functions[31] are used, markedly changed values are obtained for the effective g factors for Yb^{171}, viz., $g_s^z/g_s^+ < 1$, whereas there are only small changes for W^{183} and Tm^{169}.

ACKNOWLEDGMENTS

The advice of Dr. P. Duwez on metallurgical problems, Dr. R. Willens's suggestions related to the levitation-melting technique, and the many discussions with Dr. E. Seltzer on the interpretation of the results are gratefully acknowledged. We thank Dr. F. Boehm for the generous hospitality of the Nuclear Spectroscopy and Solid State Group. One of us (B.P.) gratefully acknowledges partial financial support from the Swedish Government's Council for Atomic Research.

[25] P. Sparrman, T. Sundström, and J. Lindskog, Arkiv Fysik **31**, 409 (1966).
[26] C. Günther and E. Kankeleit, Phys. Letters **22**, 443 (1966).
[27] W. Henning, P. Kienle, E. Steichele, and F. Wagner, Phys. Letters **22**, 446 (1966).
[28] A. Bohr and B. Mottelson, lecture notes on Nuclear Structure and Energy Spectra, Copenhagen, 1962, Chap. V (unpublished).
[29] Z. Bochnacki and S. Ogaza, Acta. Phys. Polon. **27**, 649 (1965).
[30] S. G. Nilsson (private communication).
[31] S. G. Nilsson, Kgl. Danske Videnskab. Selskab, Mat. Fys. Medd. **29**, No. 16 (1955).